sciendo

TRANSACTIONS ON AEROSPACE RESEARCH
eISSN 2545-2835, VOL. 275, NO. 2/2024, 66-92
DOI: 10.2478/tar-2024-0012

Łukasiewicz
Institute
of Aviation

FLOW SIMULATION-BASED METHODOLOGY FOR REDUCING THE RISK OF FUEL FIRE IN AN AIRCRAFT`S FUEL SYSTEM ENCLOSURE

Janusz Sznajder 0000-0003-3478-490X
Łukasiewicz Research Network – Institute of Aviation,
Al. Krakowska 110/114, 02-256 Warsaw, Poland

ABSTRACT

This study applies advanced computational fluid dynamics (CFD) simulations to enhance the safety of an aircraft's fuel system by striving to minimize the risk of on-board fire hazards. Employing a detailed flow simulation model, this research assesses the efficacy of newly designed measures within a fuel system, designed for a modified radial engine on a test-bed AN 2 airplane. The model simulates internal airflow, droplet particle flow, the formation of Eulerian Wall Film, and the vaporization process from the fuel film within the enclosure of the aircraft's equipment bay. By exploring both the original and modified geometries of this fuel system enclosure, the simulations provide insights into the flowpaths of leaking fuel, the spatial and temporal distribution of fuel vapor concentrations, and the overall effectiveness of design modifications aimed at rapid removal of hazardous substances. Structural improvements, including the addition of strategic ventilation inlets and outlets, are proposed based on the simulation results to ensure rapid dispersion of vapors and minimal residual fuel, effectively reducing the potential for vapor ignition. This study thus underscores the potential of precise CFD modelling in identifying risks and developing robust fire hazard mitigation strategies in aviation fuel systems.

Keywords

flow simulations; phase change; Eulerian wall film.

1. INTRODUCTION

Airplane on-board fuel systems can be potential sources of leaks which, due to the vaporization of fuel, may create conditions conducive to vapor ignition and the outbreak of on-board fires. This risk may be compounded by the proximity of elements of different systems, including fuel and electric systems, within the same space due to design constraints. This paper examines such a problem, based on the example of re-designed fuel and ignition systems of a piston radial engine mounted

* Corresponding Author. Email address: janusz.sznajder@ilot.lukasiewicz.gov.pl
Received 20.01.2023 • Revised 29.11.2023 • Accepted 11.04.2024
© 2024 Author(s). Article category: research article

CC BY NC ND

OPEN ACCESS

on a test-bed AN-2 airplane. In this case, the simple, carburettor-based fuel system was replaced with a more complicated system supporting fuel injection, including more elements, especially electric pumps, and having more junctions than the previous system. To minimize the risk of fire, the adopted approach involves drawing out any leaking fuel and effectively ventilating the compartment containing the fuel system (known as the fuel system enclosure or equipment bay) to prevent build-up of a volume of vapor in concentrations above the Low Flammability Level (LFL).

The design and location of the investigated fuel system limited the scope of applicable modelling approaches for addressing fuel leaks and vapor removal to Computational Fluid Dynamics (CFD) methods. This limitation arises because analytical approaches for assessing vaporization rates and vapor transport above spilled liquids are primarily designed for conditions with undisturbed airflow above the vaporizing spill and are significantly impeded by geometric obstacles present in the domain. This conclusion is supported by the review of analytical approaches in [1] and by the work in [3], which presents a method for considering the effects of walls around a spill. Unfortunately, the analytical approach for modelling vaporization in a ventilated vessel lacks generality with respect to geometric constraints in the domain.

At the present stage of advancement, CFD methods, particularly numerical solutions of the Reynolds-Averaged Navier-Stokes (RANS) equations, are well-suited for simulating both steady and unsteady flows in complex domains, including multi-phase flows and phase changes. Numerous examples of such works are listed in [2]. An example of the CFD approach to minimizing the fire hazard from a leaked flammable gas is presented in [4]. One of the problems considered is the identification of flow stagnation zones in the complex ventilated enclosure domain of a gas turbine at an electric power station, where gas originating from a high-pressure leak may accumulate. The adopted CFD techniques effectively computed local flow velocities around the turbine and provided visualization of regions with high concentrations of leaked gas. A dedicated methodology for computing the "mean age" of air at every point in the domain is also presented, which effectively solved the posed problem.

Another example of a CFD simulation of multi-phase flow, in this case including phase change, is given in [5]. This work describes two validation tests of a phase change model employed in ANSYS software (CFX and Fluent), involving the flow of a mixture of air and water vapor condensing on a cooled wall. The experiments and numerical tests involved the operation of a safety system in a nuclear containment building. In the two numerical tests, the phase change was simulated using simplified two-dimensional and three-dimensional models consisting of three flow domains: one for flow with phase change, the second for heat conduction in cooled metal walls, and the one for the flow of cooling water. These tests aimed to validate the phase change model. The effects of different mesh densities and solution convergence levels on the phase change rate and condensate mass flow were

investigated. An important conclusion stemming from the tests is that the solution shows good convergence with respect to grid size, as well as low dependence of the determined phase change rate on grid size. The solution for phase change rate obtained on grid five times sparser than the grid at the threshold of grid independence differed by only 7% from the grid-independent solution. The difference with respect to experimental results was larger, with an approximately 20% underestimation of the phase change ratio. It was noted, however, that a similar difference was reported by another CFD study [6], and the reason for this could involve higher turbulence levels in the actual flow, a value that was not available for the authors of the CFD analysis.

The methodology applied in the present work is an extension of the methodologies presented in references [4] and [5]. Vaporizing fuel is introduced into the computational domain, comprising elements of the airplane fuel system, as droplets using the Discrete Particles model of ANSYS Fluent. The fuel droplets that reach the floor of the compartment form a Eulerian Wall Film, which is driven by gravity force and tangential stress exerted by the airflow towards drainage outlets. The Eulerian Wall Film model is coupled with a phase change model, which determines the vaporizing mass. The fuel vapor is one of the species (along with oxygen and nitrogen) transported in the domain.

2. MATERIAL AND METHODS

Description of the existing drainage and ventilation system of the equipment bay

Certain elements of the fuel system are located in the equipment bay (fuel system enclosure) situated under the floor of the pilot cabin, which is marked in Fig. 1 with a red, dashed line. The complete fuel supply system also includes tanks in the upper wings and elements under the engine cowling, which were outside the scope of the present work. The location of the elements of the existing equipment bay ventilation system is shown in Fig. 1.

As shown in Fig. 1, the existing drainage and ventilation system of the equipment bay consists of an inlet A, two larger outlets with fairings, B and C, near the front bulkhead of the bay, and two smaller outlets with fairing E and D in the bottom surface, near the rear bulkhead. The larger inlet with scoop in front of inlet A exclusively serves the cabin ventilation and is not available for the ventilation of the equipment bay. The arrows F and G indicate the location of two pairs of 2 mm-diameter drainage holes in the skin of the fuselage, located on each side of the symmetry plane, in front of two bulkheads of the structure, which are intended to allow collected fluids to flow out of the bay.

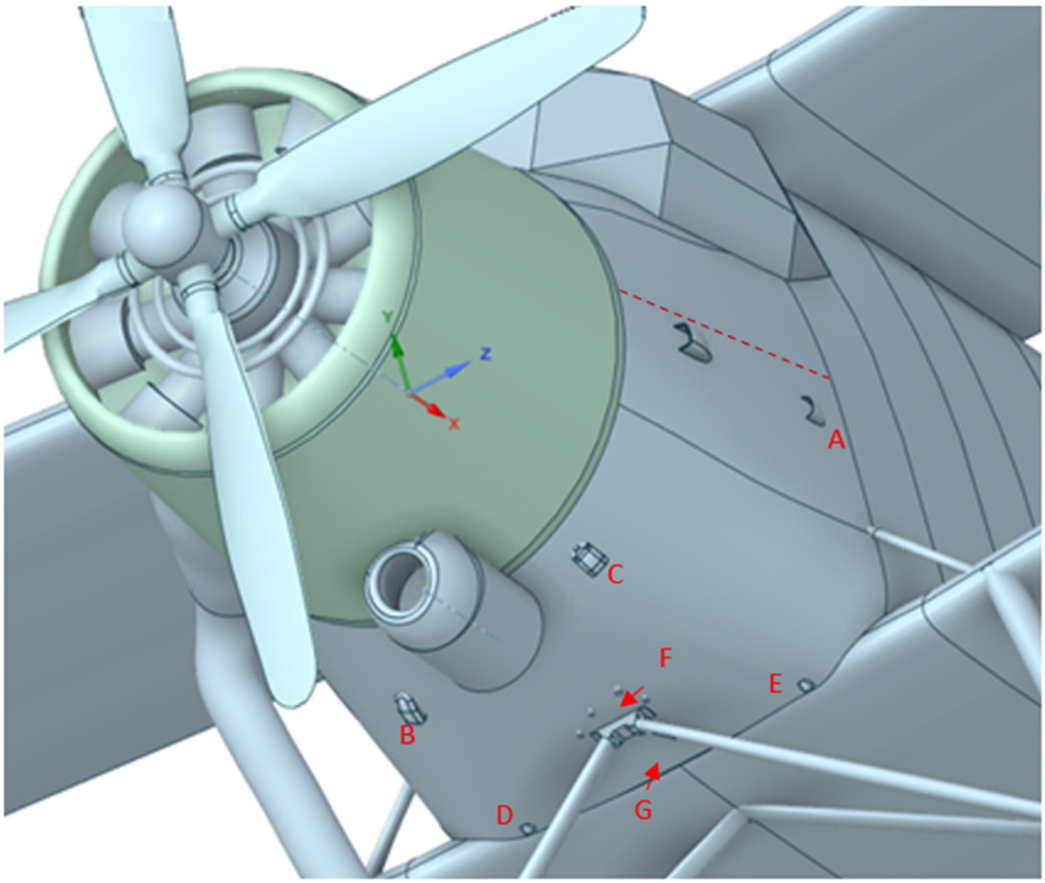


Fig. 1. Elements of the existing ventilation system of the equipment bay:
A-inlet; B,C- front outlets covered with fairings; D,E-rear outlets covered with fairings;
F,G – location of two pairs of small drainage holes, invisible in the drawing scale.

Fire hazard minimization strategy

The strategy adopted for minimizing fire hazard due to fuel leaks consisted of:

a) Identifying potential locations of leaks,
b) simulating multi-phase flow in the equipment bay, including airflow, liquid flow (fuel) and gas flow (vaporized fuel),
c) determining and tracking changes over time in the paths of leaking fuel, the distribution of fuel vapor concentrations, and the total mass of vaporized fuel inside the equipment bay,
d) designing and introducing structural modifications, including additional inlets of air and outlets for liquid and gas, and also minor modifications to the equipment bay floor to facilitate smooth outflow of leaking fuel and avoid dangerous concentrations of fuel vapor.

It was assumed that the most dangerous location for potential leaks was between the last two bulkheads of the equipment bay, where the electric-driven starter/reserve fuel pump is located. This space is shown in Fig. 2. The worst-case scenario could occur if the fuel vapor concentration rose above the flammability limit (1.5% volume fraction). In such a case, the vapor might be ignited by sparks from the commutator of the electric motor driving the fuel pump, or from the connections of the electric batteries. This pump, powered by an electric motor, operates primarily during engine start. After engine start, it may serve as a reserve pump, in case of failure of the main pump located close to engine, outside of equipment bay.

Based on the designers' experience with the volume of a possible leak in given location, the maximum value of mass flow of the simulated leak was set to 2% of the maximum mass flow generated by the starter/reserve fuel pump, or 2.6 g/s.

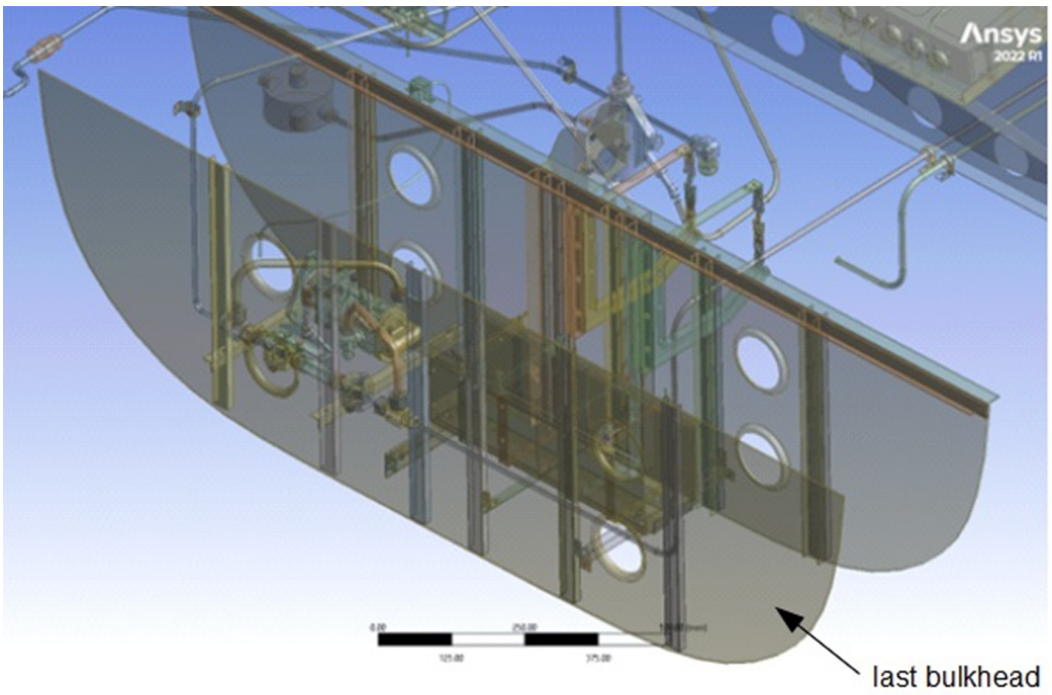


Fig. 2. Space between two last bulkheads of the equipment bay (fuselage skin and cabin floor absent for clarity, view from the rear side). Electric fuel pump on the left, electric battery pack to the right.

In the event of a fuel leak, the desired scenario of for minimizing the fire hazard should facilitate removing the rapid removal of liquid fuel reaching the bottom surface of the bay, with minimal wetting of the surface. Moreover, it should also ensure the removal of fuel vapor without creating regions of vapor concentration above the flammability limit near the potential ignition sources.

The flow and phase-change model

The flow and phase-change simulations were conducted using the ANSYS Fluent solver, incorporating specific sub-models for different phenomena: Species, Discrete-Particle Model (DPM) and Eulerian Wall Film (EWM) model. The Species model provides the physical properties of gases (oxygen, nitrogen, fuel vapor) and of liquid fuel. The Discrete Particle Model (DPM) makes it possible to model input of the leaking fuel into the computational domain in the form of discrete particles. The input details of DPM include the coordinates of injection points, droplet diameter, direction and cone angle of the stream. After the droplets reach the bottom surface of the equipment bay, they form an Eulerian Wall Film (EWF). This is driven by gravity and the tangential stress on the upper film surface exerted by the airflow. The EWF model is coupled with the phase change model, which determines the evaporation rate and makes it possible to track the vapor flow inside the domain. In the present study, the Diffusion-Balance phase change model was used with standard settings.

The species applied in the simulations included air components (O_2 and N_2), liquid fuel, and fuel vapor. The properties of the aviation fuel AVGAS 100LL applied in the simulations (most importantly: the dependence of partial pressure of fuel vapor on temperature) were not available in the solver database, and were adopted from the literature [1], [8], [9] and used in over-writing the data for iso-octane (C_8H_{18}) from the ANSYS material database. The dependence of fuel vapor partial pressure on temperature was estimated based on the formula:

$$p = \exp\left\{\left[0.7553 - \frac{413.0}{T+459.6}\right] S^{0.5} \log_{10}(RVP) - \left[1.854 - \frac{1042}{T+459.6}\right] S^{0.5} + \right.$$
$$\left. + \left[\frac{2416}{T+459.6} - 2.013\right] \log_{10}(RVP) - \frac{8742}{T+459.6} + 15.64 \right\} \quad (1)$$

from ref. [8], where:

- p is the fuel vapor partial pressure, [psi];
- RVP is Reid Vapor Pressure, [psi], defined by the norm ASTM D5191;
- T is temperature in °F;
- and S is the slope of distillation curve in °F per percent of evaporated fuel at 10% evaporated fuel (for aviation fuels 2.0, for auto-moto fuels 3.0).

The flow simulation of gas species was conducted using the ANSYS Fluent URANS solver with the k-omega SST turbulence model. As far as the Eulerian Wall Film model is concerned, the Fluent solver determines the surface distribution of the thickness and velocity of liquid film from the conservation equations for mass, momentum, and energy [10]:

$$\frac{\partial \rho_l h}{\partial t} + \nabla_s \cdot \left(\rho_l h \vec{V}_l \right) = \dot{m}_s, \tag{2}$$

$$\frac{\partial \rho_l h \vec{V}_l}{\partial t} + \nabla_s \cdot \left(\rho_l h \vec{V}_l \vec{V}_l + \overrightarrow{D_V} \right) = -h \nabla_s P_L + \rho_l h \overrightarrow{g_\tau} + \frac{3}{2} \vec{\tau}_{fs} - \frac{3\mu_l}{h} \vec{V}_l + \vec{\dot{q}}_s + \vec{\tau}_{\theta w}, \tag{3}$$

$$\frac{\partial \rho_l h T_f}{\partial t} + \nabla_s \cdot \left(\rho_l h T_f \vec{V}_l + \overrightarrow{D_V} \right) = \frac{1}{c_p} \left[\frac{2k_f}{h} \left(T_s + T_w - 2T_m \right) + \dot{q}_{imp} + \dot{m}_{vap} L \right]. \tag{4}$$

In equations (2)-(4), ρ_l is liquid density, [kg/m^3]; h is film thickness, [m]; ∇_s is surface gradient; $\vec{V}_l$ is the average fluid velocity, [m/s]; $\dot{m}_s$ is the film mass source, [kg/s]. $\overrightarrow{D_V}$ is the advection tensor, accounting for parabolic distribution of velocity in the film, p_L is pressure exerted on the film, [Pa]; $\vec{\tau}_{fs}$ is viscous stress on the gas-liquid border, [Pa]; $\vec{\tau}_{\theta w}$ is tension due to collection or separation of droplets, [Pa]. $\dot{q}_{imp}$ is the heat produced by slowing down the droplets, [J/s]; L is the latent heat of phase change, [J/kg].

Determination of airflow through the equipment bay

It was assumed that the most critical conditions for the ventilation of the equipment bay occur during the engine start and warm-up procedure, when the airplane is standing on the ground and the ventilation of the bay is achieved solely due to external flow produced by the propeller. Due to the lack of actual geometry for the propeller, its geometry, as well as the geometry of the airplane, were re-created by three-dimensional scanning of the test-bed airplane.

The thrust obtained from the Fluent model of the running propeller on a stationary airplane was validated by comparison with the estimated thrust produced by two other four-blade-propellers from report [11], the first designated 5868-R6 with an R.A.F.6 airfoil and the second designated 5868-9 with a CLARK-Y airfoil. The thrust computed with CFD (using the Moving Reference Frame) for the scanned propeller under test conditions (stationary airplane, n=700 rotations/min) was 8% lower than the thrust estimated for the first propeller and 3% lower than that estimated for the second propeller. It was concluded that the propeller model obtained from 3D-scanning of the actual propeller could be used for simulating the airflow in the vicinity of the airplane without a significant risk of overprediction of dynamic pressure.

Simulating airflow through the equipment bay induced by the airplane propeller presents a challenge due to the presence of objects of varying sizes within the same domain, influencing the flow. These include the airplane fuselage, a large object, as well as a large number of smaller elements of various airplane systems, including elements of the fuel system in the equipment bay. A computational mesh resolving all these objects would require a large number of cells. Therefore, it was decided that the computational model would consist of three sub-models:

1. A "big" model encompassing a mesh for the external domain, shown in Fig. 3, including the geometry of the airplane with the running propeller, the frontal part of the engine bay, the fuselage with inlets and outlets to the equipment bay, the wings, and the tail surfaces. This mesh covered a semi-spherical domain within 50 meters from airplane, with the plane located at its centre. The purpose of this model was to determine the pressure and velocity field around the airplane, in order to use them as boundary conditions for smaller models.
2. "Intermediate" models encompassing the external geometry of fuselage, wings, tail and undercarriage, as well as the geometry of the equipment bay and elements located therein, shown in Fig. 4. These models had their inlet surfaces located between the propeller and engine cowling, defined as a pressure-inlet boundary condition with distributions of total pressure and turbulence intensity as computed earlier using the "big" external geometry model. The boundary conditions applied on the side and rear wall included velocity inlet and pressure outlet. The "intermediate" model had variants for the baseline geometry and geometry with modified inlets and outlets of the equipment bay. The models described in points 1 and 2 were used solely for simulations of airflow (one-phase) in order to determine conditions on inlets and outlets of the equipment bay and mass flow through the bay. The models described in points 1 and 2 had approximately 15 to 20 million cells.
3. "Small" models dedicated to simulations of flow in the equipment bay, including fuel leaks and flow of fuel vapor, containing internal elements, as shown in Fig. 5. These models were prepared for testing different variants of inlets and outlets and comprised only the interior of the equipment bay, with the boundary conditions of "pressure inlet" and "pressure outlet" applied on the inlet and outlet surfaces of the particular inlet and outlet openings, as shown in Fig. 1 and Fig. 6. The values of flow variables applied as boundary conditions were determined earlier using the models described in point 2. Because the computational domain was limited to the inside of the equipment bay, the meshes were of moderate sizes (several millions elements), which made it possible to simulate the time-development of leaks, including the formation of the wall film of liquid and the flow of vaporized fuel.

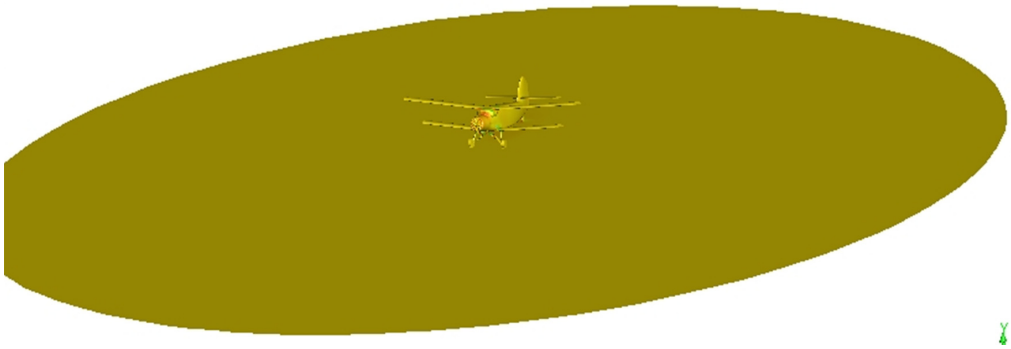


Fig. 3. Domain included in the model for the external geometry.

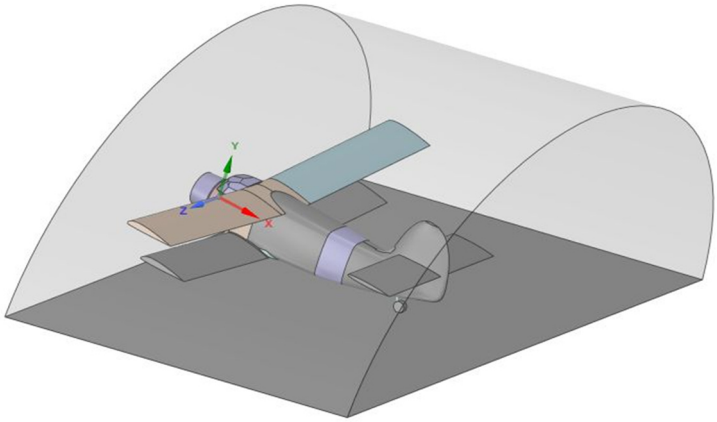


Fig. 4. Domain included in an "intermediate" model.

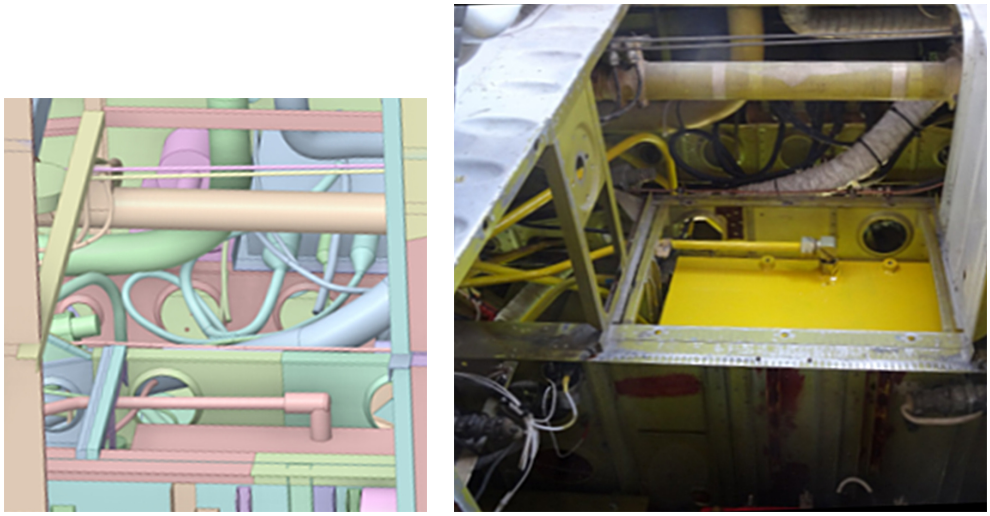


Fig. 5. Details of the systems present in the models comprising equipment bay, used for determination of mass flow and pressure values on inlet and outlet surfaces, obtained by 3D scanning (left) and photographed (right).

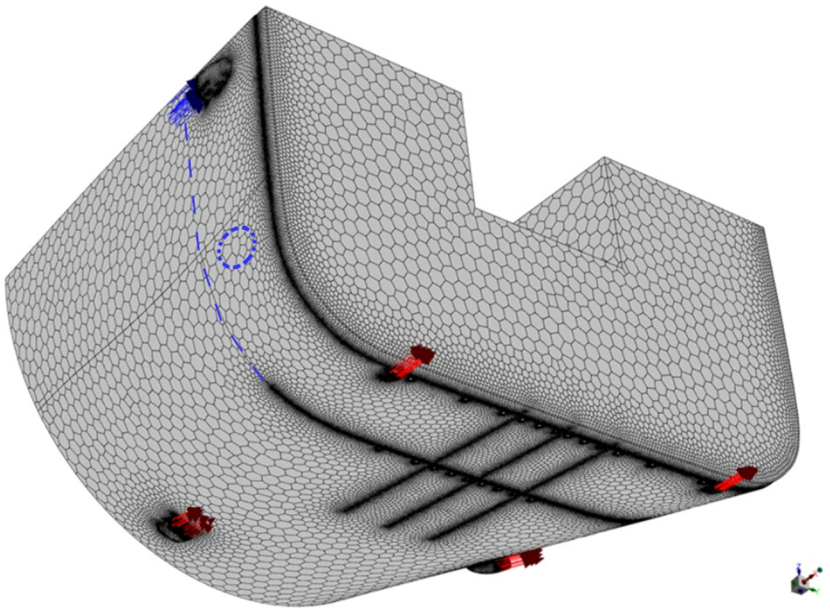


Fig. 6. Boundaries of the equipment bay, view from outside. Positions of surfaces with inlet and outlet boundary conditions indicated by blue and red arrows. Blue dashed ellipse indicates the position of additional inlet used in mesh-independence test.

3. RESULTS AND DISCUSSION

Assessment of the sensitivity of fuel and vapor removal results to mesh density

Due to limitations of computational time, the degree of sensitivity of the results of fuel drainage and removal of fuel vapor to the mesh density was analyzed within a domain of approximately one-third the volume of the equipment bay: the volume between the two last bulkheads, which for this purpose was separated from the rest of the bay by a fictitious wall surface. The position of the dividing bulkhead is indicated with blue dashed line in Fig. 6. This volume had two inlets of air, one already existing, and another introduced in the project, whose position is indicated by blue ellipse in Fig. 6. This volume had two outlets of fluid and gas, the ones visible in Fig. 6 near the rear bulkhead. The bay floor at the juncture with bulkheads was modified with a step preventing sidewise spill of the fuel, visible in Fig. 7. This feature was introduced during the present study and was absent in the baseline version of the bay. The meshes used in this investigation were prepared in the Fluent Meshing tool, operating in the classic mode, which has the option of scaling the mesh size field (the set of all parameters defining the number and distribution of mesh nodes). The size field was defined by such parameters as minimum and maximum element sizes on the given surface, the element growth ratio, and definition of the boundary layer associated with the given surface. The crudest mesh was defined with maximum

and minimum element sizes on the largest surface of 44.5 and 0.17mm, respectively a growth ratio of 1.2, and first boundary layer element height of 0.1mm. For increasing mesh density the size field was scaled by factors of 0.9, 0.8 and 0.75 applied to the size field, which resulted in mesh sizes of 1.5 million, 1.9 million, 2.36 million, and 2.5 million elements.

In order to simplify the modelling of the fuel film in this part of the study, the modelling of droplet flow was omitted. Instead, the fuel film originated from a predefined zone in the floor of the bay, shown in Fig. 7, where appropriate source terms for the fuel film were defined. The film was then driven by gravity and airflow towards the closest outlet. The film flux was set to 0.77g/s (approximately one-third of the value considered for the full bay), at which value the fuel film mass and its vaporization rate stabilized within several seconds. In Fig. 8 the change in time of film mass is shown for four mesh densities. Results indicate that while its mass stabilizes in time in each case, the stable values for denser meshes are lower than ones obtained for less dense meshes within the tested range. A possible explanation for this result is the increasing accuracy in determining the surface area covered by the film, achieved with smaller surface elements.

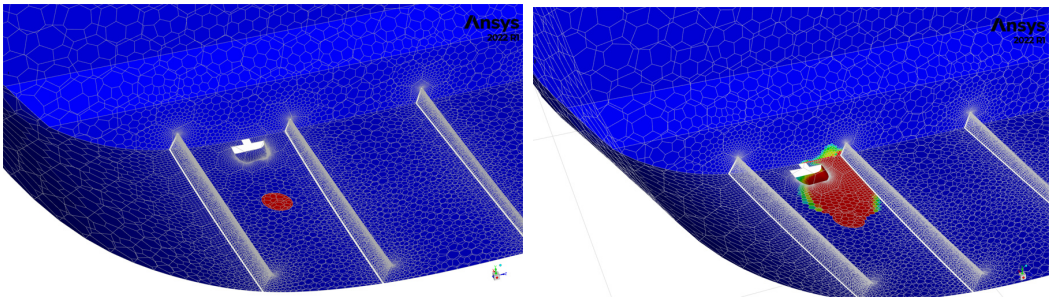


Fig. 7. Location of source zone for fuel film (left) and development of the fuel film after approximately 10 seconds (right).

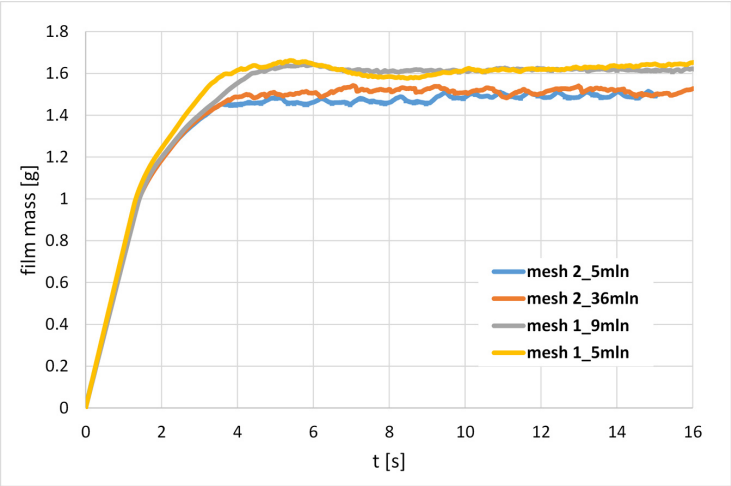


Fig. 8. Change of film mass in time after start of simulation of fuel film flow.

Figure 9 shows the change in vaporization rate for different mesh densities. As the mesh density increases, the maximum vaporization rate first increases, then decreases to a value close to that obtained for the smallest mesh. The changes are within approximately 22% of the maximum value, whereas the total mesh size changes by 40% of the maximum size. Figure 10 presents the mass of vapor collecting inside the bay as result of difference between the vaporization rate and outflow flux through the ventilation outlets. Except for the result for the roughest mesh, the maxima for the denser meshes are very close to each other and they occur at a similar time. For meshes bigger than 1.5 mln, after reaching maximum value the vapor mass stabilizes or tends to decrease.

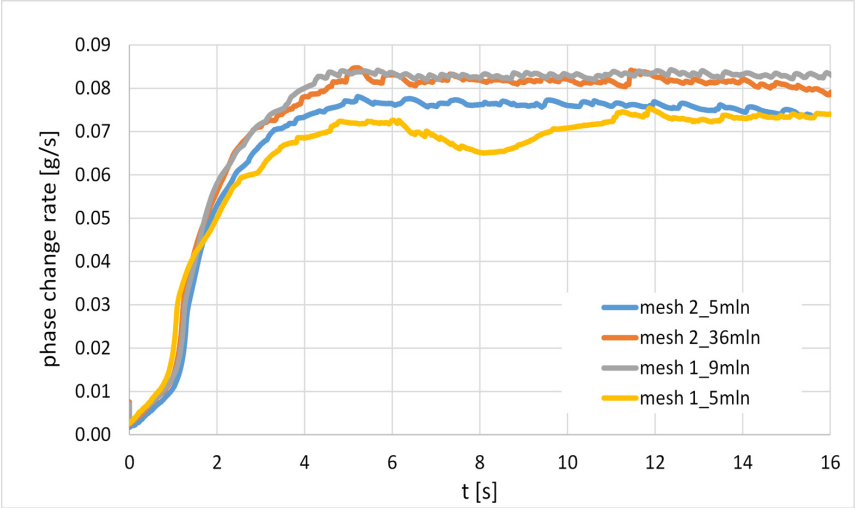


Fig. 9. Change of phase change rate over time after start of simulation of fuel film flow.

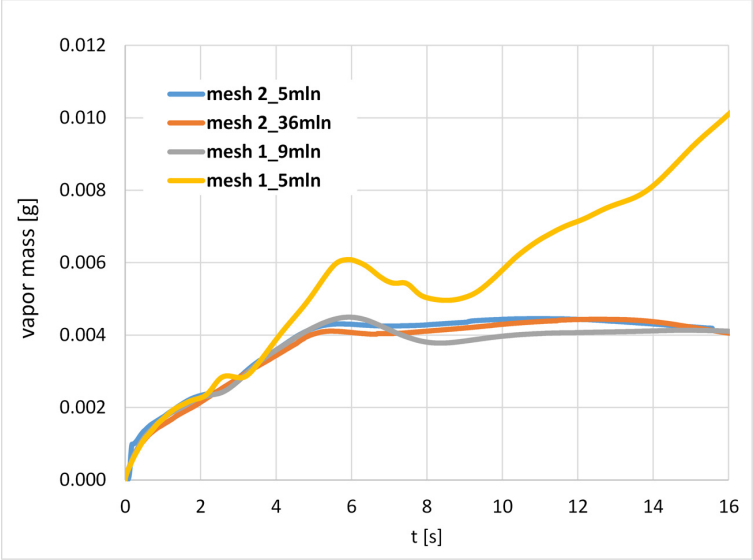


Fig. 10. Change of fuel vapor mass over time after start of simulation of fuel film flow.

The results for gas vapor collection, along with the vaporization rate and film mass development over time, indicate that for mesh densities higher than very low density used for the coarsest mesh, the investigated phenomena become qualitatively insensitive to mesh density. Most importantly, the mass of fuel vapor trapped inside the bay is relatively insensitive to mesh density. Based on results shown in Fig. 9 and Fig. 10 it was decided that mesh density corresponding to 2.36 million elements was sufficient for further simulations of the fuel vapor flow in the full volume of the equipment bay.

Regarding the sensitivity of the vapor parameters inside the equipment bay to the mesh density in the external domain, the most important potential effects concern the influence on the pressure difference between the inlets and outlets of the bay. A decreasing pressure difference may worsen the ventilation of the bay and may lead more gas vapor to be trapped inside it. Therefore, it was decided to skip simulations with varying external grid densities and to directly investigate the effect of a decreasing pressure difference driving the internal flow on the removal of fuel vapor from the bay. The reduced pressure difference was achieved by lowering pressure values at the boundary condition surfaces, which were reduced by 30% and 50% from their nominal values (164 Pa of total pressure at the inlets and -60 Pa of static pressure at the outlets). These changes in pressure difference were significant, and should exceed the effects of local pressure dependence on the external mesh density. The simulation results, shown in Fig. 11, indicate a rather moderate influence of the inlet-outlet pressure difference on the mass of the trapped gas. Closer inspection of this phenomenon revealed that the primary cause of this reduction was a decreasing vaporization rate, which accompanies the airflow at decreasing pressure difference between the inlets and outlets, as shown in Fig. 12. In Fig. 13, in turn, also demonstrates that the fuel vapor outflow rate is proportional to the vaporization rate.

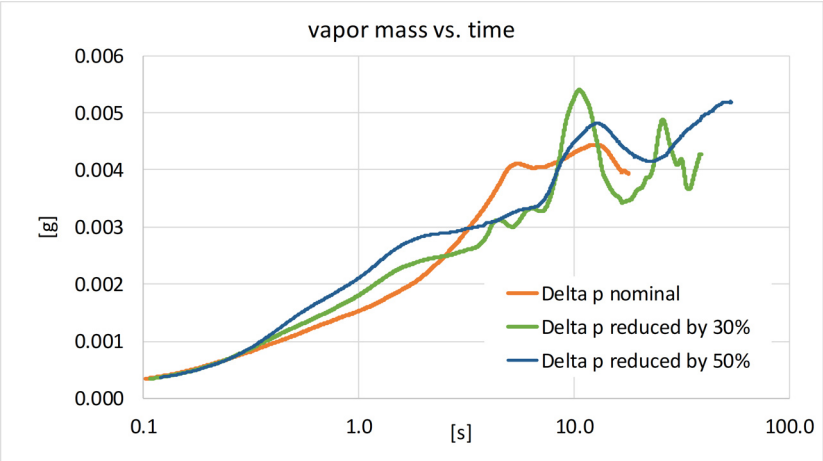


Fig. 11. Change over time in fuel vapor mass trapped inside the bay at decreasing pressure difference between its inlets and outlets.

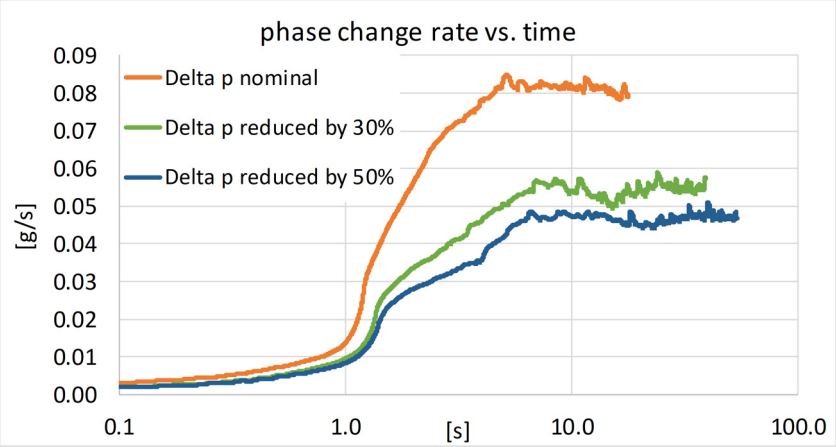


Fig. 12. Change over time in fuel vaporization rate at decreasing pressure difference between its inlets and outlets.

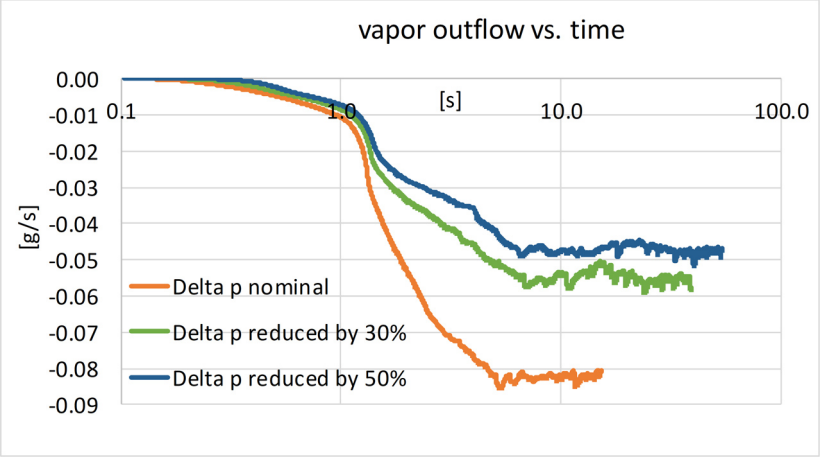


Fig. 13. Change over time in fuel vapor outflow mass rate at decreasing pressure difference between its inlets and outlets.

Results of the airflow simulations for the baseline ventilation case

The first stage of flow simulation for the full baseline bay involved achieving quasi-steady airflow conditions in the equipment bay after flow initiation, before initializing the DPM model and simulations of fuel film flow and vaporization. Flow simulations conducted for the case with a stationary airplane in the large domain (mesh types 1 and 2) produced the following values of pressure on inlet and outlet surfaces and air mass flow through the equipment bay:

Table 1: Pressures on inlet and outlets (relative to operating pressure 101325 Pa) and values of air mass flow.

	inlet A	outlet C	outlet B	outlet E	outlet D
total pressure [Pa]	164.29				
static pressure [Pa]		-56.89	-40.03	-57.27	-52.60
air mass flow [kg/s]	3.6124e-2	1.667e-2	1.2259e-2	3.864e-3	3.1346e-3

The pressure values presented in Table 1 were determined on an "intermediate" model as surface-averaged values on the respective inlet and outlet surfaces and applied as boundary conditions for simulations of fuel leak and phase change. The leak source was set at a point located under a connection of elements chosen in consultation with the designers. It was modelled as an injection point of a stream of discrete particles using the Discrete Particle Model of ANSYS-Fluent. The droplets had a pre-defined diameter of 1 mm, and were subject to 1g acceleration, influenced by the airflow in the bay.

After quasi-steady airflow conditions were reached, the Discrete Particle Model was activated and droplets began to be injected into the domain. Upon reaching the floor surface, the droplets turned into an Eulerian Wall Film and moved along the floor of the bay. The transition of the droplets into the Eulerian Wall Film at 2s after the start of leak simulation is shown in Fig. 14. The fuel mass flow of the simulated leak was 2.6 g/s (approximately 2% of the electric pump's capability).

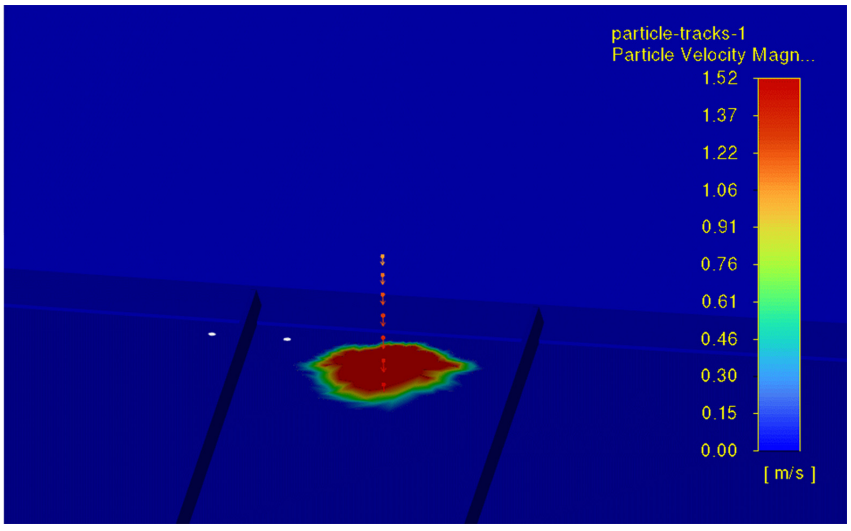


Fig. 14. Instantaneous transition of stream of fuel droplets (discrete particles) into Eulerian Wall Film at 2 seconds after the start of simulations of the leak. The scale pertains to particle velocity magnitude, while the colours of the fuel film are indicative of wetted fraction of a surface cell. View from front towards the last bulkhead.

The development over time of the area wetted by the fuel film is shown in Fig. 15. The fuel film can be seen to spread towards the sides of the equipment bay along the surface of the last bulkhead.

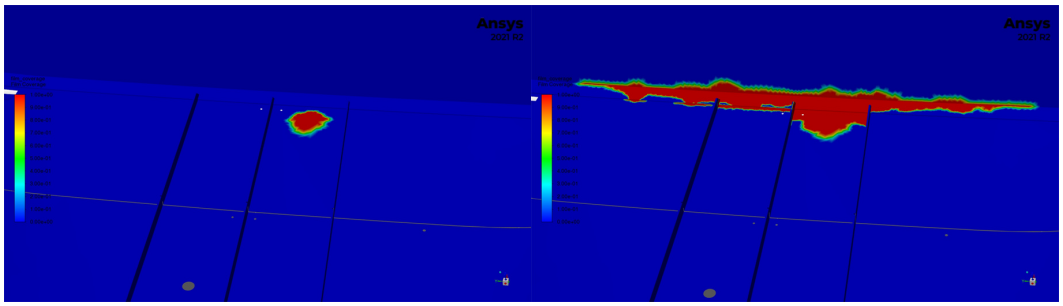


Fig. 15. Change in the film-wetted surface area between t=2s and t=68s of simulation. The view is from the upper front of the bay. For good visibility only the floor and the last bulkhead are shown.

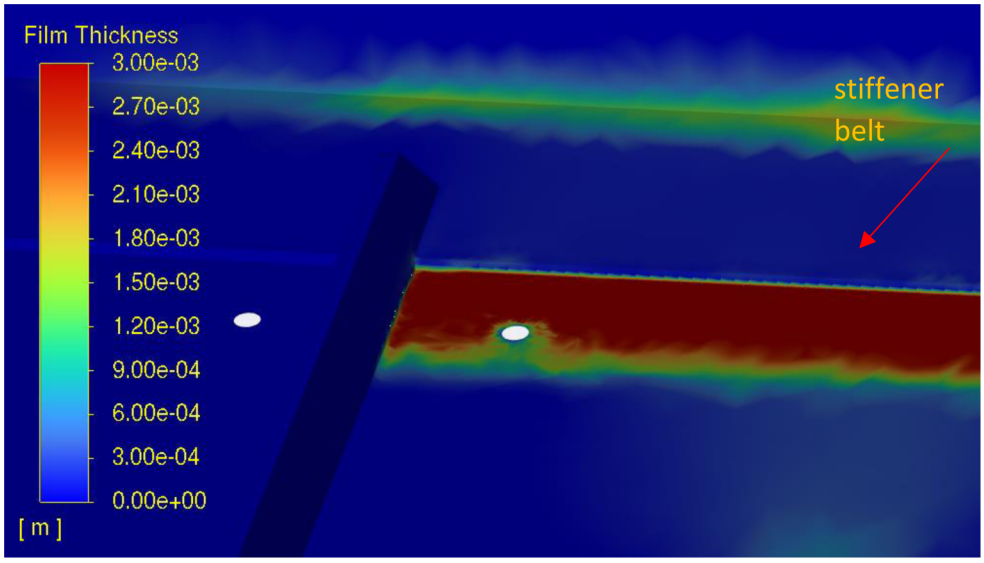


Fig. 16. Distribution of film thickness near outlet holes at t=10s of simulation

Results of the simulated, approximately 68 second-long flow of leaked fuel show steady growth of the mass of fuel trapped inside the equipment bay. The wetted area grows toward the surface of the last bulkhead, and then sidewise. The reason for this flow direction is visible in Fig. 16, where the profile of the bottom surface of the equipment bay is shown in the form of a colour map. It can be seen that: a) the outlets of the bay are located at a distance (approximately 5cm) in front of the last bulkhead, due to presence of a stiffener belt, approximately 2-3 mm thick (indicated also in Fig. 15), b) that the central bottom surface is sloped downwards in the direction of the fuselage length, and c) the central part of the bottom surface is several mm below the level of outlets located at its sides. This causes part of the

leaked fuel to be trapped inside the bay, which then vaporizes. The growth over time of the mass of trapped fuel liquid and trapped fuel vapor is presented in Fig. 17.

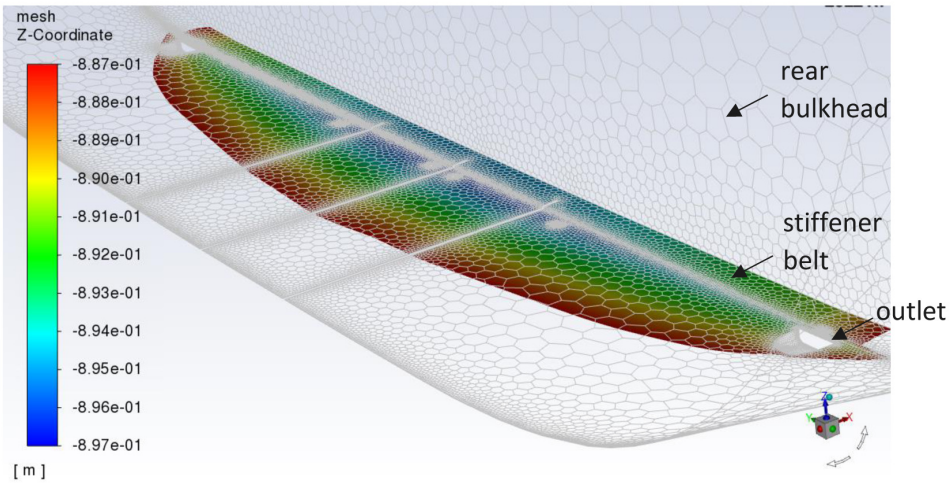


Fig. 17. Profile of the bottom surface of the equipment bay near the last bulkhead. The round holes in the bottom surface are enlarged versions of the drainage holes shown in Fig. 15, introduced in the later phase of the work.

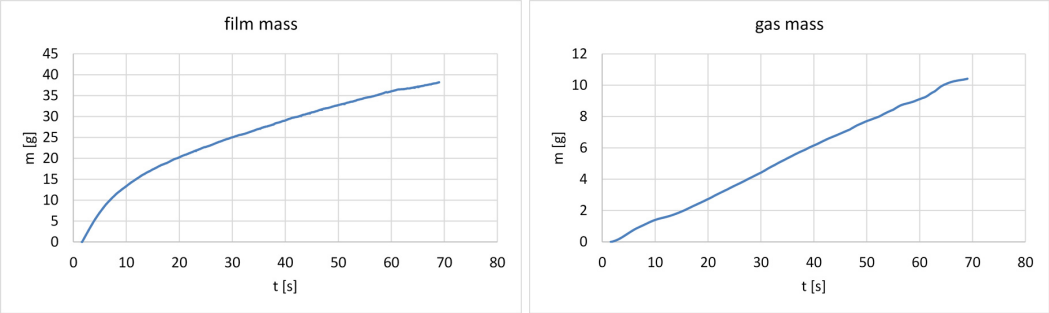


Fig. 18. Changes over time in film mass and mass of fuel vapor inside the equipment bay.

The steady increase in the mass of gas vapor trapped inside the equipment bay leads to a rising concentration of vapor, which locally becomes higher than the flammability level (1.4% volume ratio, 5% mass ratio). The spatial distribution of the gas concentration was obtained using the cell register functionality in the ANSYS Fluent solver, which can be used to indicate cells with a chosen variable having prescribed value or being in a prescribed range. Fig. 19 shows two cell registers, with cells of mass concentration of fuel vapor above the flammability level in two time moments. The spatial distribution of these cells is consistent with the vector visualization of airflow in the vertical plane containing the inlet to the equipment bay, presented in Fig. 20.

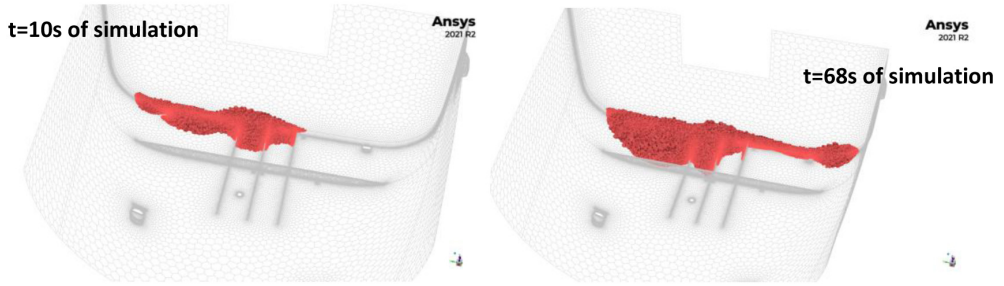


Fig. 19. Cells with fuel vapor concentration above flammability level at t=10s of simulation and at t=68s of simulation.

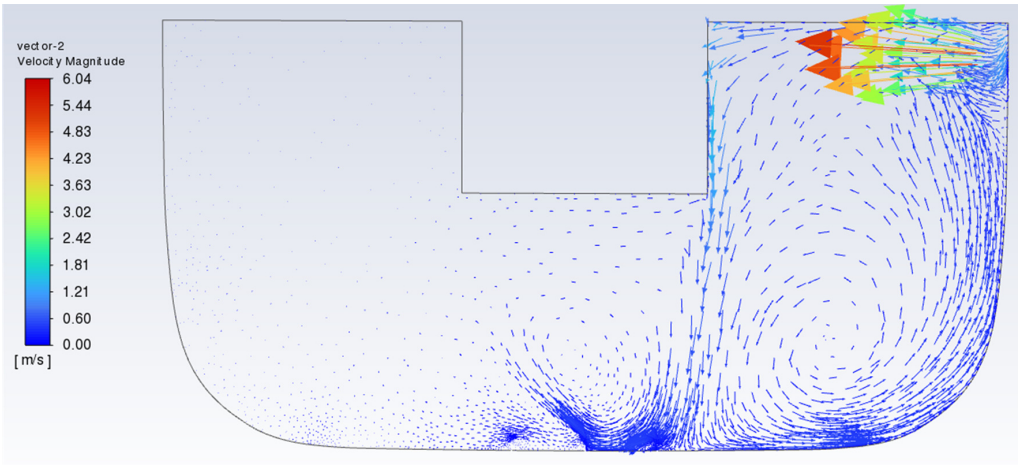


Fig. 20. Vectors of velocity in the vertical plane containing the inlet to the equipment bay.

It can be seen that – due to the location of the single ventilation inlet close to the last bulkhead, just below the cabin floor and in front of the "cavity step" in the floor – the air entering the bay almost immediately loses its energy and is directed downwards with low velocity, creating a slow-rotating vortex in the part of the bay just below the inlet, while in the other part of the bay the air is almost at a stand-still.

In order to minimize the likelihood of an on-board fire due to such a fuel leak, an improvement in ventilation and removal of liquid fuel from the bottom surface of the bay was sought. The measures to achieve this included:

- adding inlets to equipment bay,
- adding outlets with fairings,
- filling the voids at the front of the bulkhead in order to prevent collection of liquid fuel.

The position of additional inlets to the equipment bay is shown in Fig. 21. The size of the inlets was limited by the distance between stringers and framers of the fuselage. Their position was selected such that the mutual interference between them should be minimal, and they should fulfil the additional task of providing cooling air for some additional electric subsystems in the equipment bay, not mentioned in detail in this paper. Each of the additional inlets had a scoop and a stream diverter, as shown in Fig. 22. All the inlets were located on the left side of the fuselage, due to presence of large exhaust pipe, disturbing the flow, on its right side.

In order to improve removal of leaking fuel and fuel vapor, additional outlets were proposed. The computational model was created with a large number of optional outlet surfaces, which could be switched on or off by a change in the type of boundary condition on each of the surfaces. The additional outlets, visible in Fig. 23 and in Fig. 24, were 20mm in diameter. This approach was chosen in order to determine the minimum number of outlet surfaces necessary for achieving proper ventilation by means of a change in the local boundary condition in the solver, on a surface prepared for this task, rather than by means of a more time-consuming modification of the CAD model and the creation of a new computational mesh.

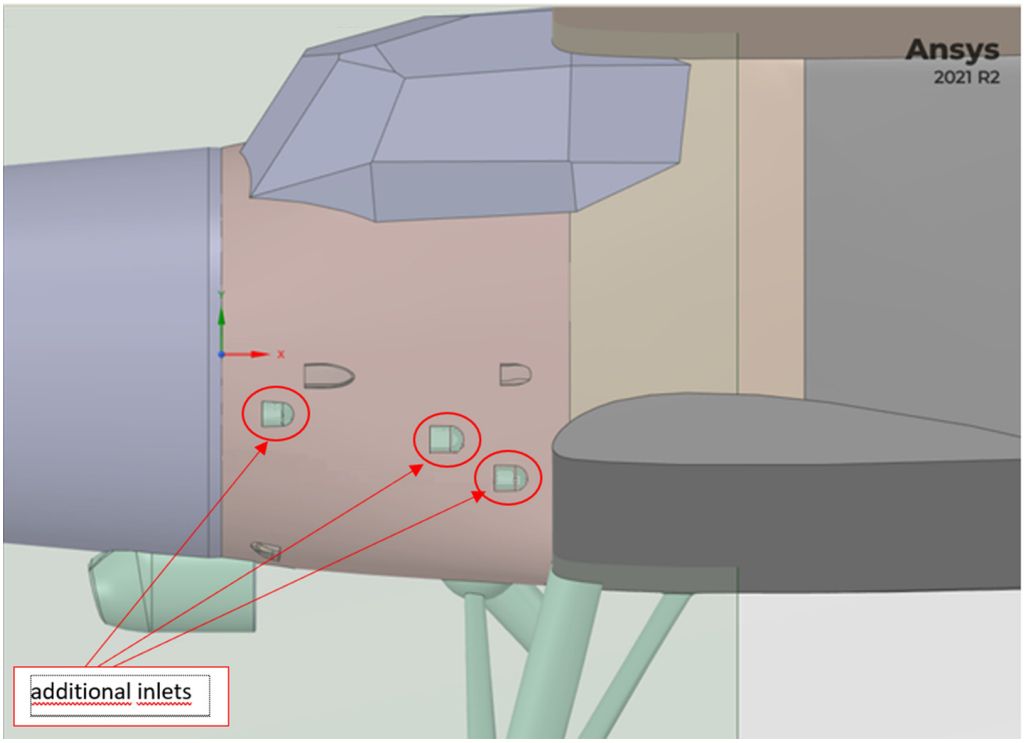


Fig. 21. Location of additional inlets ventilating the equipment bay.

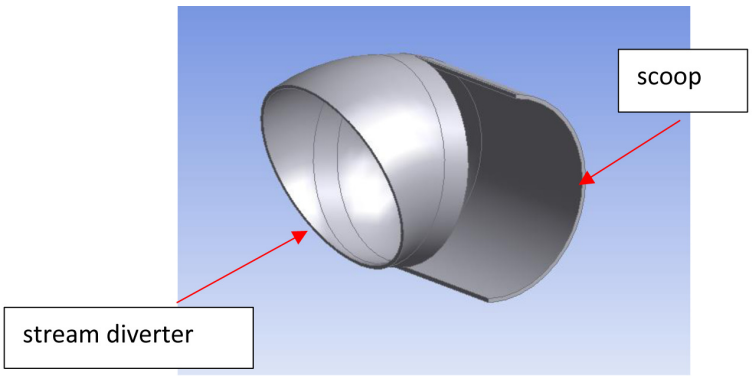


Fig. 22. Details of the geometry of the additional ventilation inlets.

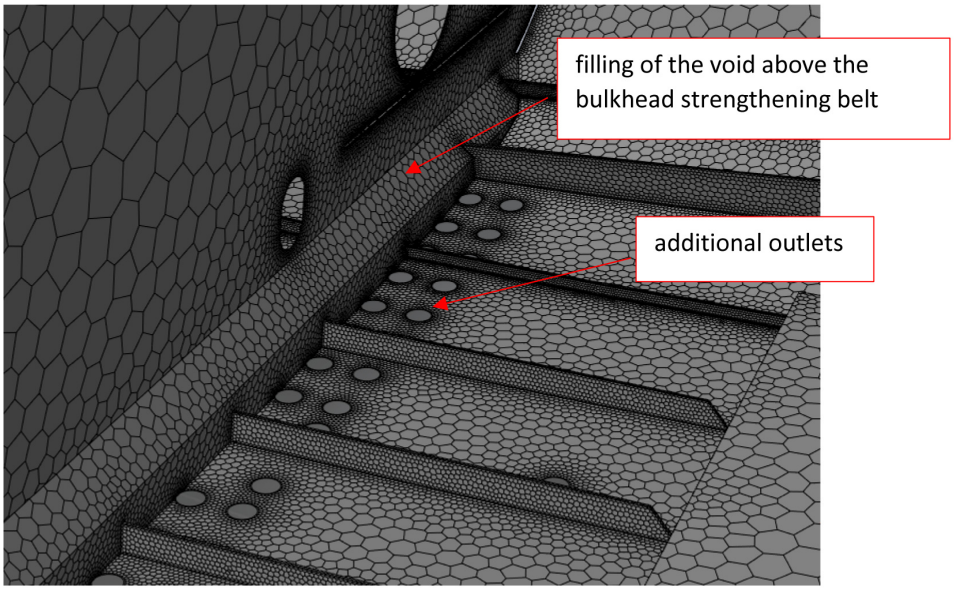


Fig. 23. View of the additional outlets from the bay and of the filling above the strengthening belt, preventing the accumulation of liquid fuel

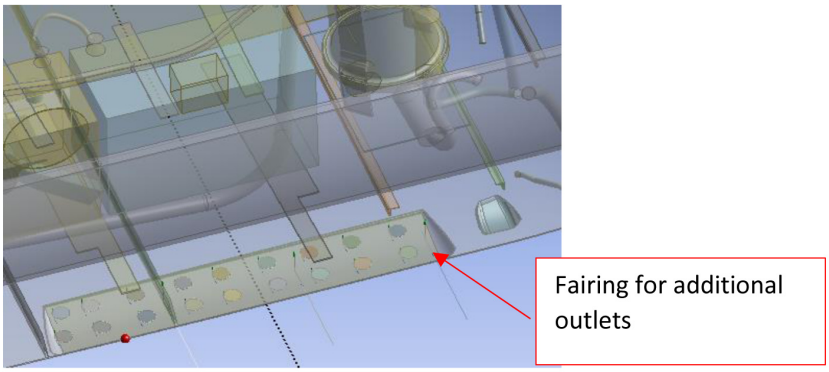


Fig. 24. Fairing for the additional outlets, obtained by scaling of the existing fairing of a small side outlet, visible to the right of the picture (view created using the surface permeability option for visualizing surfaces in ANSYS Design Modeler).

Results of the simulations for modified ventilation system

First, the results concerning the additional functionality of providing cooling, fresh air towards selected sub-systems are presented. These computations were performed on an "intermediate" model, with the computational domain both inside the bay and outside the airplane, as shown in Fig. 24. The velocity contours in cross-sections, where these elements are present, are shown in Fig. 25 and Fig. 26, as contours of the Z velocity (horizontal, negative for air moving to the right side). It can be seen that the additional inlets effectively fulfil their role. In Fig. 26, the existing, inefficient inlet is also visible, just below cabin floor.

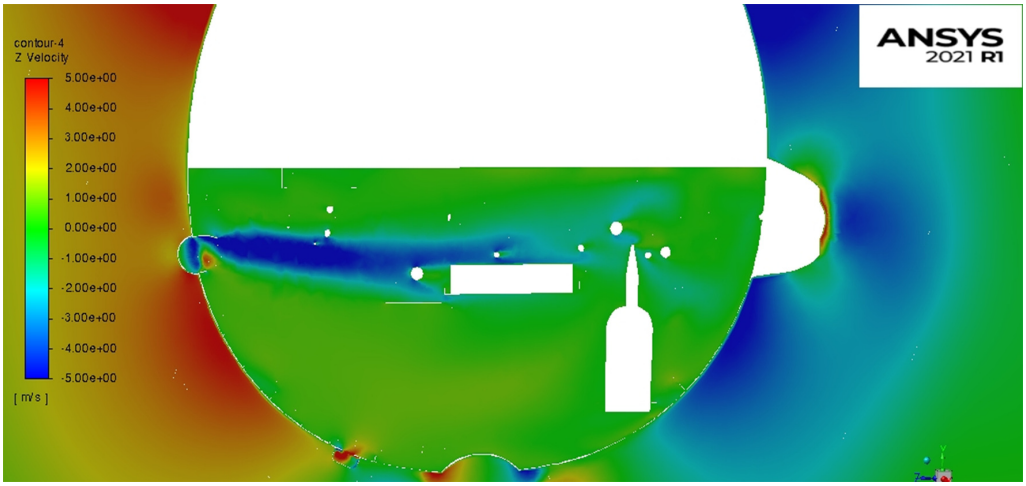


Fig. 25. Contour of velocity stream of fresh air entering the bay through the first additional inlet.

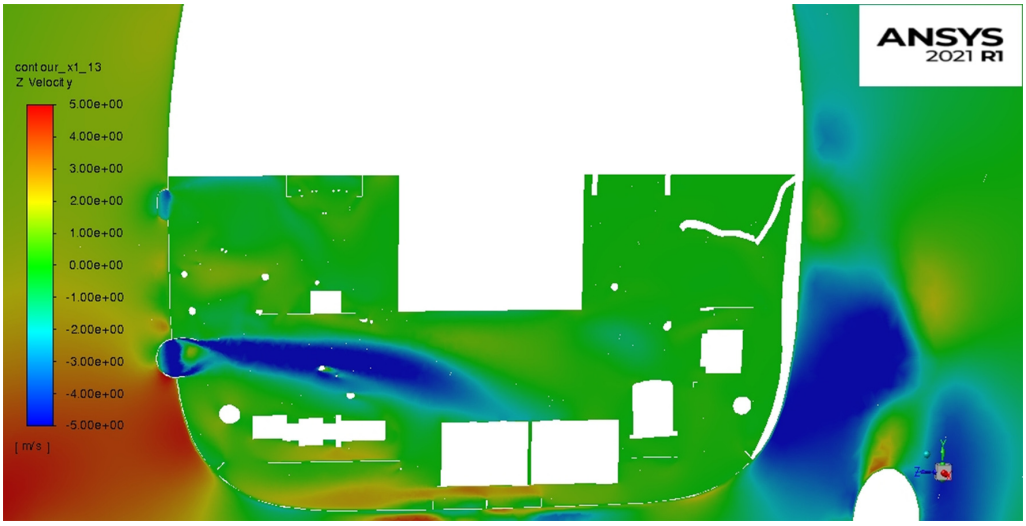


Fig. 26. Contour of velocity stream of fresh air entering the bay through the third additional inlet.

For the modified ventilation system the first run of simulations of airflow and flow of leaking fuel and its vapor was conducted with all the additional outlets active. The impact point of the droplets on the bottom surface was at the same distance from the plane of the last bulkhead, as in the first simulation for the baseline case. In Fig. 27, Fig. 28 and Fig. 29 it can be seen that the outflow of the leaking fuel and fuel vapor stabilized within a few seconds. Figure 30 presents the surface distribution of film thickness, while Fig. 31 presents spatial distribution of cells with vapor mass concentration exceeding the flammability level. It is evident that the leaking fuel is being carried away from the bay through the closest outlets, and the region of mass concentration of vapor is restricted to the very close neighbourhood of the outlets

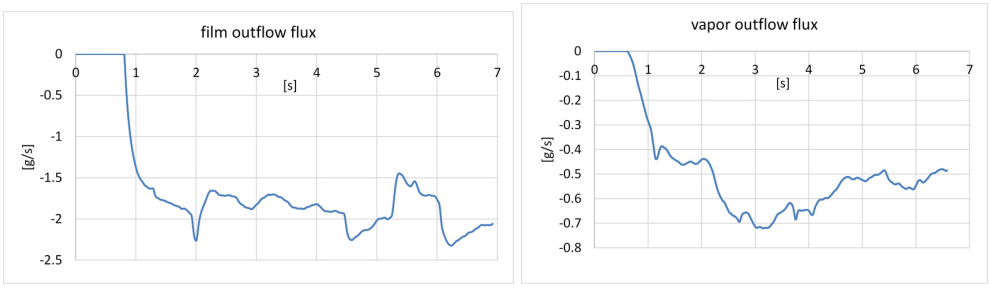


Fig. 27. Time dependence of fluxes of liquid film and fuel vapor, integrated over the surface of all outlets.

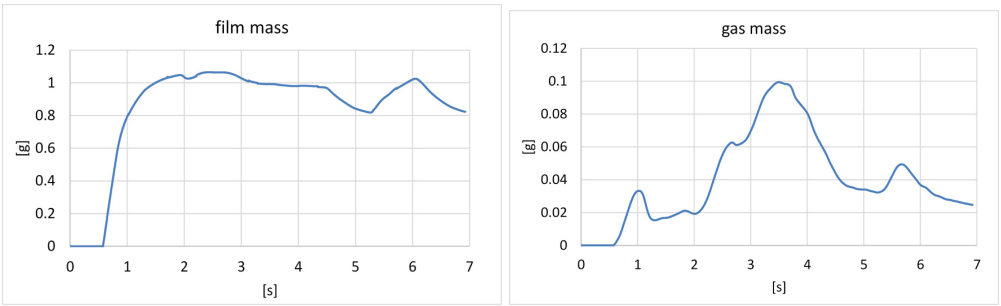


Fig. 28. Time dependence of mass of fuel film, integrated over the bottom surface, and fuel vapor integrated over the equipment bay volume.

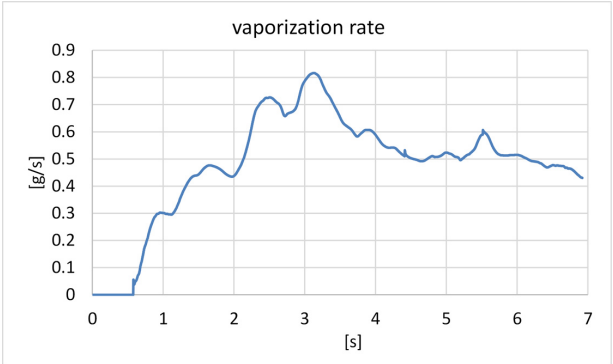


Fig. 29. Time dependence of vaporization rate, integrated over the bottom surface.

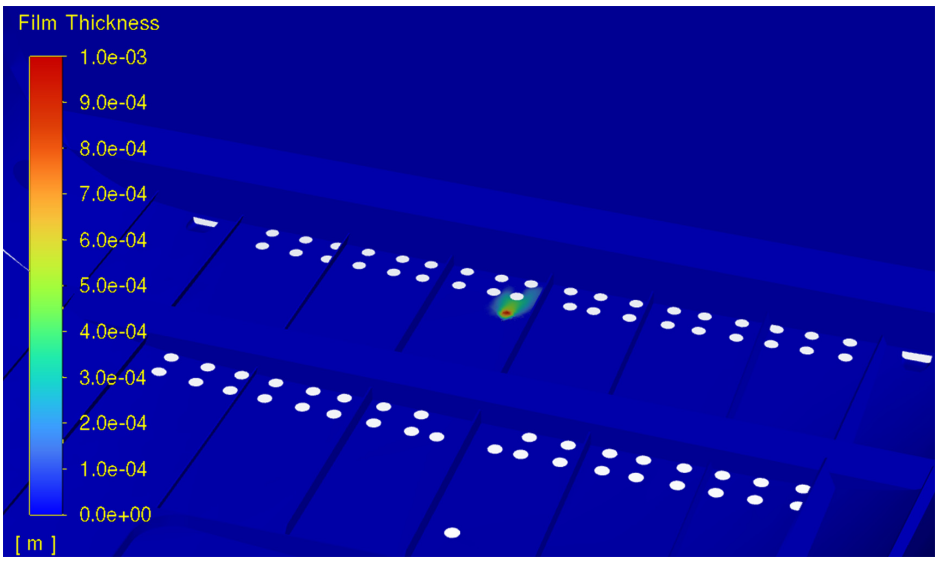


Fig. 30. Distribution of the film thickness after modification of the ventilation system. For good visibility all elements other than wall boundaries of the bay are omitted in the picture, including the fourth bulkhead

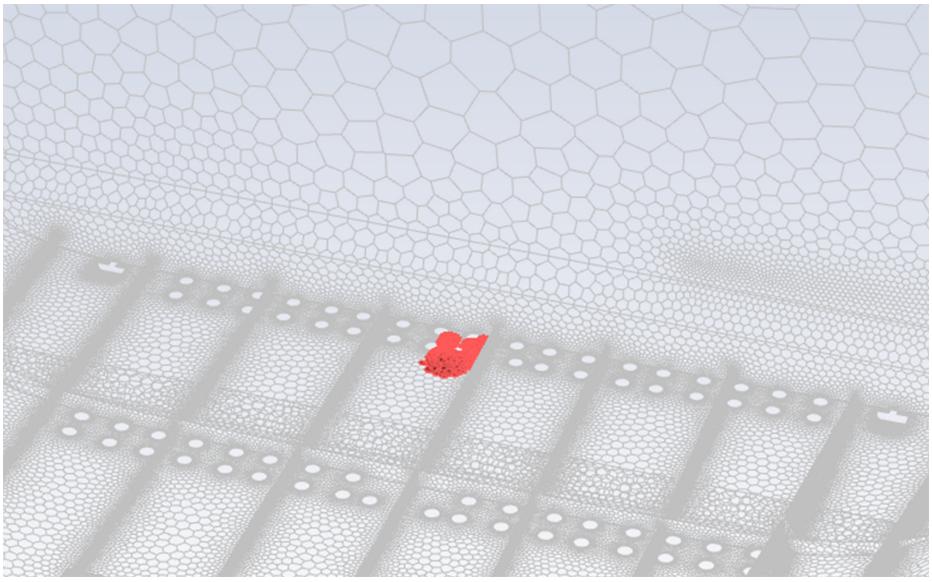


Fig. 31. Location of cells with mass concentration of fuel vapor above the flammability level. All elements other than wall boundaries omitted in the picture.

Two more stringent simulation tests were next conducted. Since perforating the bottom surface of the equipment bay would obviously decrease its structural strength, in the first of the two tests the number of additional outlets was reduced to one in each skin strip between the longitudinal stringers. In the second test, additionally, the pressure boundary conditions corresponded to the lowest rotation velocity of the propeller, 481 rpm, occurring for approximately 30 seconds during engine start and

warm-up (a decrease from 700 rpm). The approximately 15-second period of this phase was simulated, during which time the flow variables concerning the liquid fuel and vapor mass outflow, as well as the mass of fuel and vapor remaining inside the bay stabilized. The results are presented in Fig. 32 and Fig. 33. Figure 34 shows the volume cells with mass concentration above the flammability level (in red), and cells with vapor mass concentration starting from the lower value of 50% of flammability level. The visualisations were obtained for propeller rpm=481. Comparison of the two concentration patterns shows the direction where the vapor cloud may expand in the event of an increasing volume of leaking fuel. This direction is along the wall, towards other outlets.

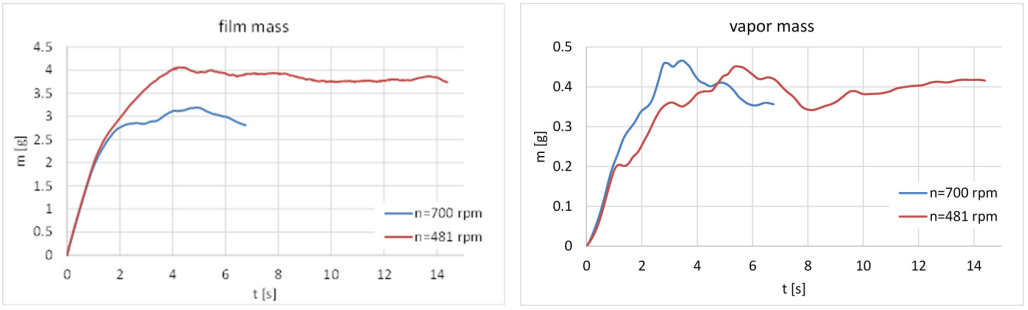


Fig. 32. Time dependence of film mass, integrated over the bay bottom surface, and fuel vapor mass, integrated over the bay volume.

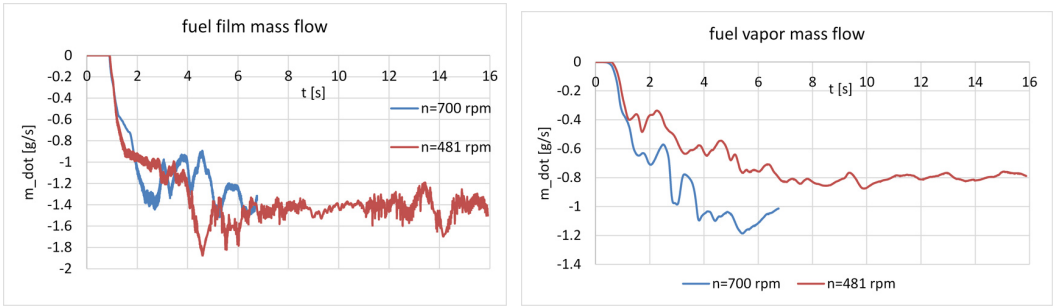


Fig. 33. Time dependence of film mass flow and fuel vapor flow, summed over the outlets.

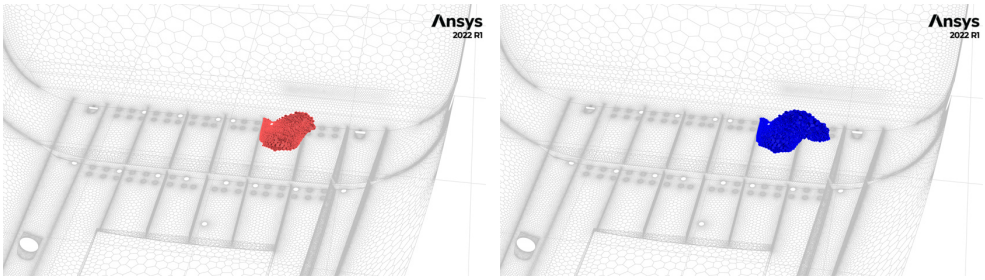


Fig. 34. Left: visualization of cells with mass concentration of fuel vapor above the flammability level; right: visualization of cells with mass concentration of fuel vapor above the concentration of 50% of the flammability level. The visualisations were obtained for propeller rpm=481.

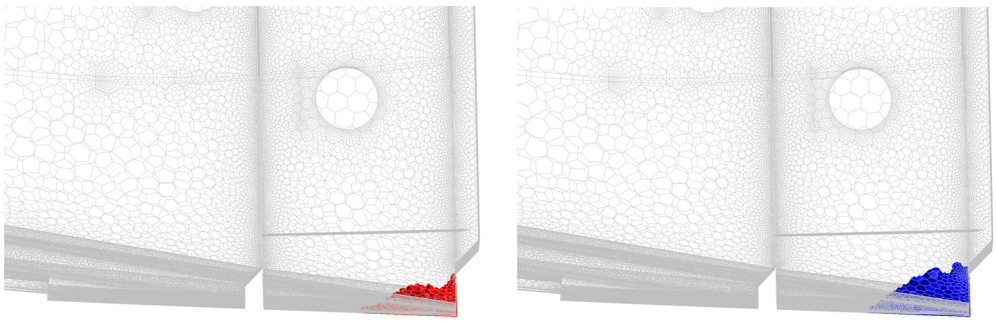


Fig. 35. Side view of distribution of cells shown in perspective view in Fig. 27.

Discussion of results and future directions

The simulations of the flow and phase change in the equipment bay indicate that the modification most crucially needed is the elimination of zones of where liquid fuel originating from leaks in connectors of the elements of the fuel system may collect and vaporize. This may be achieved by creating sloped fillings above the strengthening belts of the bulkheads and adding additional openings in the floor, shielded by external fairings against backflow of air. These modifications are relatively easy to fabricate, however, they might necessitate additional considerations regarding the structural strength of the surfaces involved. Additional modifications include air inlets which could direct the airflow inside the bay towards the proper outlets in the floor, preventing the circulation of a mixture of air and fuel vapor inside the bay. The presence of longitudinal stringers in the floor of the bay favours fuel film flow towards the outlets. Additionally, the fact that fuel vapor is heavier than air aids in its removal through the proposed outlets.

The proposed structural modifications need to have their effectiveness verified in real working conditions. For safety reasons, this may be carried out without spilling inflammable fluids. The flow pattern of leaking fluid may be visualized with dyed water, and this technique should verify the elimination of places where fluid collects before exiting the bay, while air velocity can be effectively measured by sensors, such as thermo-anemometric sensors, situated at points of interest. Much as for the liquid fluid flow pattern, the flowpaths of gas in the bay can be verified by a smoke-visualisation technique.

Regarding the simulation techniques, the combination of the Discrete Particle Model with Eulerian Wall Film and Phase Change modelling, as used herein, has been shown to offer a convenient and effective solution for modelling of leaks of arbitrary origin, which may be easily changed in space without modification of the computational mesh. The wall film model only operates on surface elements of the mesh and is therefore a very effective modelling technique, faster than Volume of Fluid, which may serve as an alternative, but requires a locally dense volume mesh to resolve the height of the layer of the liquid and its flow. However, the development

of the film flow and vapor flow over time is a process that consumes computational time and memory, which restricted the number of cases analysed.

4. CONCLUSIONS

In summary, this study has effectively demonstrated the utility of computational fluid dynamics (CFD) simulations in enhancing the safety protocols of aircraft fuel systems. Utilizing a robust flow simulation model developed in the ANSYS Fluent environment, this research facilitated the design and verification of modifications aimed at mitigating fire risks associated with fuel leaks in an aircraft's fuel system enclosure (equipment bay). The model solves the Unsteady Reynolds-Averaged Navier-Stokes (URANS) equations to simulate the multiphase dynamics of air, gasoline vapor, discrete fuel particles, and the Eulerian Wall Film, along with phase transitions between liquid and gas states.

The simulations not only confirmed the effectiveness of the proposed structural adjustments – such as additional air inlets and outlets and local reshaping of the compartment floor – but also provided quantitative insights into the reduction of high-concentration fuel vapor zones near critical electrical system components. By focusing on the expedient removal of leaked fuel and its vapors, the study offers practical design solutions that significantly diminish the likelihood of vapor ignition. Future work will aim to implement these modifications in real-world conditions to verify their practical efficacy, using non-flammable simulants to ensure safety during testing.

Overall, these findings underscore the critical role of detailed flow modeling in developing reliable fire hazard mitigation strategies and contribute to ongoing advancements in aircraft design safety.

Acknowledgement

The author is grateful to the people who helped him in the research: the INNOVAR 3D company, who did the 3D scanning of the aircraft and its systems, the SYMKOM company – ANSYS partner in Poland for providing helpful examples for setting-up the phase-change model, and to colleagues from Institute of Aviation: Wieńczysław Stalewski, Andrzej Iwaniuk and Tomasz Kwiatkowski for comments, providing computational data and preparation of computational meshes.

REFERENCES

[1] Pénelon T, Debuy V, Truchot B, Wagner C, Donnat L, Lechaudel JF. Pool evaporation: Experimental tests at medium-scale with gasoline. J Loss Prev Process Ind [Internet]. 2020;65(2020):104072. Available from: https://doi.org/10.1016/j.jlp.2020.104072

[2] Galeev A, Ponikarov S, Salin A. Numerical simulation of evaporation of volatile liquids. J Loss Prev Process Ind [Internet]. 2015;38:39-49. Available from: https://doi.org/10.1016/j.jlp.2015.08.011

[3] Tamanini F. Explosive volume formation from the release of vapors or liquids in enclosures. Fire Saf Sci Proc Seventh Int Symp Fire Saf Sci [Internet]. 2003:247-58. Available from: https://doi.org/10.3801/IAFSS.FSS.7-247

[4] Heynes OR, Clutter JK. Assessing explosion hazards in gas turbine enclosures. In: 49th AIAA Aerospace Sciences Meeting including the New Horizons Forum and Aerospace Exposition, 4-7 January 2011, Orlando, Florida [Internet]. 2012. Available from: https://doi.org/10.2514/6.2011-527

[5] Zschaeck G, Frank T, Burns AD. CFD modelling and validation of wall condensation in the presence of non-condensable gases. Nucl Eng Des [Internet]. 2014;279:137-46. Available from: https://doi.org/10.1016/j.nucengdes.2014.03.007

[6] Ambrosini W, Forgione N, Oriolo F, Dannoehl C, Konle HJ. Experiments and CFD analyses on condensation heat transfer on a flat plate in a square crosssection channel. In: 11. International Topical Meeting on Nuclear Reactor Thermal-Hydraulics (NURETH 11); 2005 Oct 2-6; Avignon, France.

[7] Hemighaus G, Boval T, Bacha J, Barnes F, Franklin M, Gibbs L, Hogue N, Jones J, Lesnini D, Lind J, Morris J. Aviation Fuels Technical Review [Internet]. Chevron Products Comapny; 2006. Technical Report. Available from: https://www.chevron.com/-/media/chevron/operations/documents/aviation-tech-review.pdf

[8] US EPA [Internet]. AP 42, Fifth Edition, Volume I Chapter 7: Liquid Storage Tanks | US EPA; 2020 Jun [cited 2023 Nov 29]. Available from: https://www.epa.gov/air-emissions-factors-and-quantification/ap-42-fifth-edition-volume-i-chapter-7-liquid-storage-0

[9] Compton TJ. Flight Performance Testing of Ethanol/100LL Fuel Blends During Cruise Flight [Internet]. Waco: Baylor University; 2008. Available from: https://baylor-ir.tdl.org/server/api/core/bitstreams/06e27a1a-6d13-4180-9aca-4c629791a8a6/content

[10] Ansys Fluent Theory Guide [Internet]. U.S.A.: ANSYS, In; 2021. Available from: https://dl.cfdexperts.net/cfd_resources/Ansys_Documentation/Fluent/Ansys_Fluent_Theory_Guide.pdf

[11] Hartman EP, Biermann D. The Aerodynamic Characteristics of Full-Scale Propellers Having 2, 3, and 4 Blades of Clark Y and R.A.F. 6 Airfoil Sections [Internet]. NACA; 1938 Jan. NACA-TR-640. Available from: https://ntrs.nasa.gov/api/citations/19930091715/downloads/19930091715.pdf

[12] Bukowski J, Łucjanek W. Napęd śmigłowy. Teoria i konstrukcja [Propeller Propulsion, Theory and Design]. Warszawa: Wydawnictwo MON; 1986. [in Polish].